

Stochastic Loewner evolution driven by Lévy processes

I Rushkin, P Oikonomou, L P Kadanoff and I A Gruzberg

The James Franck Institute, The University of Chicago, 5640 S. Ellis Avenue,
Chicago, IL 60637

Abstract.

Standard stochastic Loewner evolution (SLE) is driven by a continuous Brownian motion, which then produces a continuous fractal trace. If jumps are added to the driving function, the trace branches. We consider a generalized SLE driven by a superposition of a Brownian motion and a stable Lévy process. The situation is defined by the usual SLE parameter, κ , as well as α which defines the shape of the stable Lévy distribution. The resulting behavior is characterized by two descriptors: p , the probability that the trace self-intersects, and \tilde{p} , the probability that it will approach arbitrarily close to doing so. Using Dynkin's formula, these descriptors are shown to change qualitatively and singularly at critical values of κ and α . It is reasonable to call such changes "phase transitions". These transitions occur as κ passes through four (a well-known result) and as α passes through one (a new result). Numerical simulations are then used to explore the associated touching and near-touching events.

1. Introduction

The scaling limit of many two-dimensional critical lattice models and growth models encountered in statistical physics may be described in terms of fractals. The boundaries of the Fortuin-Kastelyn clusters in critical q -state Potts models and critical percolation models, for example, in this limit are known to be fractal, conformally invariant curves [1, 2]. Stochastic Loewner evolution [3, 4] (also described as Schramm-Loewner evolution and abbreviated as SLE) is a rigorous mathematical tool for producing and studying stochastic conformally invariant curves in the plane (see Refs. [5, 6, 7, 8] for review). It was conjectured, therefore, that SLE is a description of such statistical systems. In several special cases this conjecture has been rigorously proven.

SLE is based on the Loewner equation taken from complex analysis [9]. This equation contains a driving (or forcing) function, $\xi(t)$, which determines all the properties of SLE. A few reasonable requirements constrain the choice of this function to a scaled Brownian motion, which leaves only one free parameter. One of these requirements (that the forcing function is continuous) ensures that the curves produced by SLE do not exhibit branching, thus leaving many systems, such as branching polymers, out of the picture. In this paper, we generalize SLE by dropping the demand that the forcing stochastic function be continuous, but keeping the requirement of stationary and statistically-independent increments. This leads to a much broader class of forcing processes including, in particular, the so called Lévy processes [10, 11, 12, 13]. This generalization might be a useful description of tree-like stochastic growth.

Standard SLE has been studied in various geometries under the names of chordal, radial and other kinds of SLE's. In this paper we restrict ourselves to the chordal situation (growth in the upper half plane). We believe that our generalized SLE in a radial geometry may be relevant for description of the diffusion-limited aggregation, and plan to study it in a separate publication.

In the next section, we define and describe the problem, in terms of the parameters which define the forcing. The forcing includes both a scaled Brownian motion and a stable Lévy process. The parameters are κ , which sets the normalization of the Brownian term, c which sets the normalization of the Lévy term, and α which determines its shape. This qualitative section ends with numerical simulations of the traces, the geometrical structures generated by the SLE.

The final section of the paper gives the analysis of the short-distance properties of the traces showing both analytically and numerically that the traces have qualitative change in behavior as κ and α each pass through critical values, respectively at four and one. The transition at $\kappa = 4$ is quite analogous to a well known transition in the standard SLE [4]. The latter phase transition, at $\alpha = 1$, is entirely new. This paper focuses upon the short-distance manifestations of this phase transitions in the chordal geometry. The accompanying large-scale features (which may be different for different geometries) will be the subject of a subsequent paper.

We point out that most of the statements about the behavior of objects related to SLE and its generalizations are probabilistic, and typically appended by qualifiers “almost surely” or “with probability one” in mathematical literature. We will not use these qualifiers explicitly assuming that they should be applied wherever it is necessary.

Some technical details of our calculations are given in the Appendix.

2. Description of problem

2.1. Loewner evolution

The so called chordal Loewner evolution is described by a differential equation obeyed by a function $g(z, t)$. At each value of the “time” t , this function is a conformal map from a subset of the upper half of the complex z -plane (which we refer to as the *physical plane*) to the entire half plane H (*mathematical plane*). Specifically we write

$$\partial_t g(z, t) = \frac{2}{g(z, t) - \xi(t)}, \quad g(z, 0) = z. \quad (1)$$

Here $\xi(t)$ is the forcing, mentioned above. Alternatively, the function $h(z, t) = g(z, t) - \xi(t)$ obeys

$$\partial_t h(z, t) = \frac{2}{h(z, t)} - \partial_t \xi(t), \quad h(z, 0) = z, \quad (2)$$

assuming that ξ vanishes at $t = 0$.

For any point $z \in H$ these equations are valid up to the swallowing time $\tau(z)$, which is defined as the first time when $g(z, t) = \xi(t)$ or $h(z, t) = 0$ so that the right hand sides of Eqs. (1) and (2) become singular. The *hull* of the Loewner evolution is defined as the set of all points which become singular (are swallowed) in this way up to time t . At any given time, the z 's that newly enter the hull may represent a single point or a more complicated set, sometimes including a subset H with a finite area. See Figure 1.

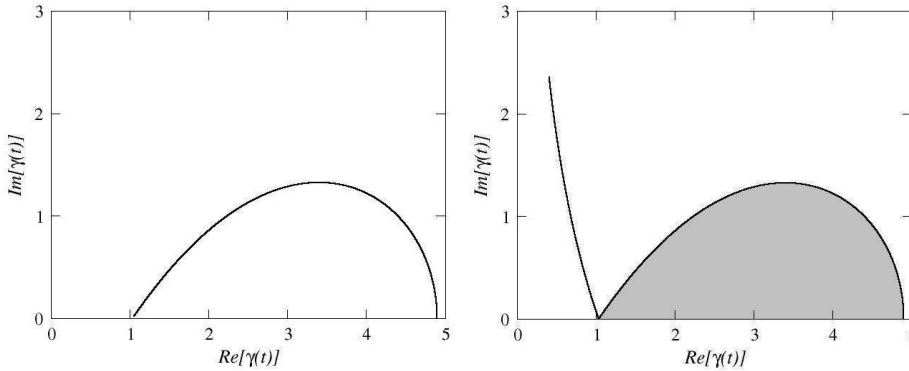


Figure 1. The trace and the hull for a touching event. Here $\xi(t) = 2\sqrt{6(1-t)}$ for $t \in (0, 1)$ and zero elsewhere [15]. Left shows the situation just before touching ($t \rightarrow 1^-$); right shows the situation just after ($t > 1$). The trace is the thick dark line. The hull consists of that line plus the grey area. That area is added to the hull at $t = 1$. Note that there is a continuum of points added to the hull at the time of touching, but only one of these is on the hull's boundary and is the point $\gamma(1)$ of the trace.

Another geometrical object considered in the SLE literature is the growing tip $\gamma(t)$ of the hull. The point $z = \gamma(t)$ is picked from among the (perhaps many) points which newly enter the hull at time t . Among these, this point is unique for having the property of being on the boundary of the hull at the time t , see Figure 1. More formally, this point is defined by [4]

$$\gamma(t) = \lim_{z \rightarrow 0} h^{-1}(z, t), \quad (3)$$

where the limit is taken within H . The union of the points $\gamma(t)$ up to a time T is the trace of the evolution up to T .

The choice of the process $\xi(t)$ defines the properties of the hull and the trace. In particular, if $\xi(t)$ has a discontinuity (jumps), branching or discontinuity occurs in the trace and the hull may become disconnected. For a sufficiently smooth $\xi(t)$ (a precise condition involves Hölder continuity, see Refs. [14, 15, 16]) the trace is a curve parametrized by t . Moreover, if the trace is a simple curve, that is a curve without double points and without touchings of the boundary, it then coincides with the hull.

2.2. The forcing

Standard SLE [3] is the Loewner evolution with scaled Brownian forcing

$$\xi(t) = \sqrt{\kappa}B(t), \quad (4)$$

where $B(t)$ is a standard Brownian motion. In physical terms this means that the “time derivative” $\dot{\xi}(t)$ is a white noise with intensity κ : $\langle \dot{\xi}(t)\dot{\xi}(t') \rangle = \kappa\delta(t-t')$. The increments of $\xi(t)$ in distinct time intervals are stationary and statistically independent. These properties of $\xi(t)$ ensure that the process $g(z, t)$ is conformally invariant in the sense that the time evolution is consistent with composition of conformal maps. In particular, the ensemble of $g(t+s)$ can be obtained by functional composition of $g(t)$ with $g(s)$, each drawn from the correct ensemble.

If we want to generalize Eq. (4) but maintain the functional composition property, we may only discard the requirement of continuity of the forcing $\xi(t)$ but keep its increments to be stationary and statistically independent. This leads to a broad class of stochastic processes, including the so called Lévy processes [10, 11, 12], also called Lévy flights in physics literature [13]. The simplest of these are the so called stable Lévy processes $L_\alpha(t)$ characterized by a single real parameter α in the range $0 < \alpha < 2$. The process $L_\alpha(t)$ is composed of a succession of jumps of all sizes. In a time interval dt , $L_\alpha(t)$ jumps by an amount between x and $x + dx$ with the probability proportional to

$$dt dx \frac{1}{|x|^{1+\alpha}}. \quad (5)$$

More precisely, the probability distribution function of $L_\alpha(t)$ is given by the Fourier transform

$$P(x, t) = \int_{-\infty}^{\infty} e^{-ikx} e^{-t|k|^\alpha} \frac{dk}{2\pi}. \quad (6)$$

The case of $\alpha = 2$, formally corresponding to a Brownian motion, is, in fact, quite different from $\alpha < 2$. We find it interesting to combine a Brownian motion with a stable Lévy process as the input to our generalized version of the SLE. Thus we choose as our forcing the function

$$\xi(t) = \sqrt{\kappa}B(t) + c^{1/\alpha}L_\alpha(t). \quad (7)$$

Every time a discontinuity of the driving force occurs the trace develops a branching point. With Lévy flights, therefore, there are infinitely many branching points on all size-scales.

The stable Lévy processes are self-similar [10]. For any positive number b the two processes, $L_\alpha(t)$ and $b^{1/\alpha}L_\alpha(t/b)$, are “equal in distribution”, that is, statistically identical, which we denote as

$$L_\alpha(bt) \stackrel{d}{=} b^{1/\alpha}L_\alpha(t). \quad (8)$$

Thus, a typical trajectory of a Lévy flight looks like many clusters separated by long jumps. Each cluster, if zoomed into, again looks like many clusters separated by long jumps, and so on [13].

2.3. Scales for SLE with Lévy flights

We choose the driving force $\xi(t)$ in Loewner evolution to be of the form (7):

$$\partial_t g(z, t) = \frac{2}{g(z, t) - \sqrt{\kappa}B(t) - c^{1/\alpha}L_\alpha(t)}, \quad g(z, 0) = z. \quad (9)$$

If $c = 0$ this process is scale-invariant [7]. The run of the Loewner evolution up to a time bt is statistically the same as the run up to a time t , rescaled by a factor of \sqrt{b} . The properties of the growing hull do not change with time except for general size rescaling. In this Brownian driving force is exceptional.

The addition of Lévy flights changes the situation: time becomes significant. Consider a time rescaling $t \rightarrow bt$, where b is a positive number. We construct the rescaled conformal map

$$g_b(z, t) = b^{-\frac{1}{2}}g(b^{\frac{1}{2}}z, bt). \quad (10)$$

It satisfies the initial condition $g_b(z, 0) = z$, and using the self-similarity property (8) we observe that g_b obeys an equation of exactly the same form as Eq. (9) except that the value of c is changed to

$$c_b = cb^{(2-\alpha)/2}. \quad (11)$$

The strength of the Lévy process flows under time-rescaling, making SLE not scale-invariant. (Many calculations in the usual SLE with pure Brownian motion are based on scale-invariance [4, 6, 7, 17] so that they cannot immediately be extended to the present case.)

This situation can be phrased in the language of the renormalization group (RG). The critical behavior of a system described by an SLE with purely Brownian forcing is determined by a fixed point of an RG. Lévy flights make the system non-scale invariant, and their addition to the forcing can be thought of as a perturbation that is relevant at the fixed point. We do not know at present what such perturbations might be in terms of microscopic models of critical systems described by Brownian SLE. One possible candidate is a long range interaction of some kind.

The flow of c has a fixed point at zero, when we recover the result that SLE with pure Brownian motion is scale-invariant. For $c > 0$, the ratio of κ and the effective c changes with time. At time $t = 1$ it is just $c_1 = c$. At time t the effective ratio of the two terms in the forcing is

$$\frac{c_{\text{eff}}^{1/\alpha}}{\kappa^{1/2}} = \frac{c^{1/\alpha}}{\kappa^{1/2}} t^{\frac{1}{\alpha} - \frac{1}{2}}. \quad (12)$$

Therefore, crossover behavior can be observed at a time

$$t^* = \left(\frac{\kappa^\alpha}{c^2} \right)^{1/(2-\alpha)}. \quad (13)$$

At small times $t \ll t^*$ the evolution is dominated by the Brownian motion, whereas at large times $t \gg t^*$ it is dominated by Lévy flights. (If κ were very large or very small one would have to consider the independent effect of the three terms in the denominator of Eq. (9), but for κ of order one this is the only crossover that need be considered.) There is a similar crossover in space at a spatial scale $x^* = \sqrt{t^*}$, with the Brownian motion dominating the small scale events.

2.4. Numerical representation of SLE

We approximate the integration of the SLE by introducing a discretized version, where each realization of $\xi(t)$ is replaced by a piecewise constant function with jumps appropriately distributed. Let X_i , $i = 1, 2, \dots$, be a sequence of real stochastic variables. We define a realization of the discretized driving force to be constant in the interval $((j-1)\tau, j\tau]$ (where τ defines the mesh on the time variable) with $\xi(0) = 0$ and

$$\xi(t) \rightarrow \xi_j = \sum_{i=1}^j X_i \quad \text{for } (j-1)\tau < t \leq j\tau. \quad (14)$$

For this forcing we can exactly solve for the trace. Within each time interval (t_{j-1}, t_j) we can solve the SLE forward:

$$g(z, j\tau) = \sqrt{[g(z, (j-1)\tau) - \xi_j]^2 + 4\tau + \xi_j}, \quad (15)$$

or backward:

$$g(z, (j-1)\tau) = \sqrt{[g(z, j\tau) - \xi_j]^2 - 4\tau} + \xi_j. \quad (16)$$

Equations (15), (16) define an infinitesimal conformal map and its inverse for each time interval j :

$$w_j(z) = \sqrt{(z - \xi_j)^2 + 4\tau} + \xi_j, \quad (17)$$

$$f_j(z) = w_j^{-1}(z) = \sqrt{(z - \xi_j)^2 - 4\tau} + \xi_j. \quad (18)$$

The trace can then be calculated numerically as an iteration process of infinitesimal conformal mappings starting from the condition $g(\gamma(t), t) = \xi(t)$ as follows [18, 19]:

$$\gamma_j = \gamma(j\tau) = f_1 \circ f_2 \circ \dots \circ f_{j-1} \circ f_j(\xi_j). \quad (19)$$

The value of ξ_j is determined by the variables X_i which are randomly drawn from the appropriate distribution according to the properties of the driving force $\xi(t)$.

In Figures 2–9 we show typical SLE traces for different types of driving force up to a time T . For Figures 2–3 we have set $c = 0$ and used increments drawn from Gaussian random variables in order to show SLE traces for the standard case of Brownian noise. The noise realization for these two pictures is the same, multiplied by an appropriate κ . As is well known [4],[7], the trace does not touch itself for $\kappa \leq 4$, but does so for $\kappa > 4$. The figures show these contrasting behaviors.

For Figures 4–5 we approximate SLE with Lévy flights using the method in [20]. As expected, these figures show branching structures produced by the discontinuous jumps. The figures suggest that a forcing consisting solely of discontinuous jumps does not produce any self-intersections.

Figures 6–9 show the combined effects of jumps and Brownian motion. Exactly the same noise realizations have been used as in the previous four figures. The different sources of change in X (Brownian and Lévy) have simply been added to one another.

Comparison between Figures 6–9 and 2–5 exemplifies the crossover behavior discussed in the previous section. Take for example Figure (4). The trace consists of branches which look like the ones produced by the Loewner equation with constant forcing. Whenever a jump occurs, a new branch starts growing off some point on the trace or the real axis. If now we add Brownian noise to the driving force (Figures 6–9) the trace at the largest scales makes branches like in the case with only Lévy flights. However, if we zoom in (see insets) the trace appears similar to the SLE trace with only Brownian forcing (Figures 2–3).

3. Analysis of short-distance behavior

3.1. Phases of SLE

It is well known [4] that the standard Brownian SLE process is qualitatively different in its behavior in the three different intervals $0 < \kappa \leq 4$, $4 < \kappa < 8$, and $8 \leq \kappa < \infty$. In the first interval the SLE trace forms a fractal that neither touches itself nor the real line (see Figure 2). In the second interval the trace touches itself and the real line (see Figure 3). For large enough time it will touch down arbitrarily far from the origin. Eventually it will surround and swallow up any point on the real line no matter how far it is from the origin. In the third, all points on the real line are surrounded sequentially, but also the trace fills in all the surrounded areas. This kind of behavior

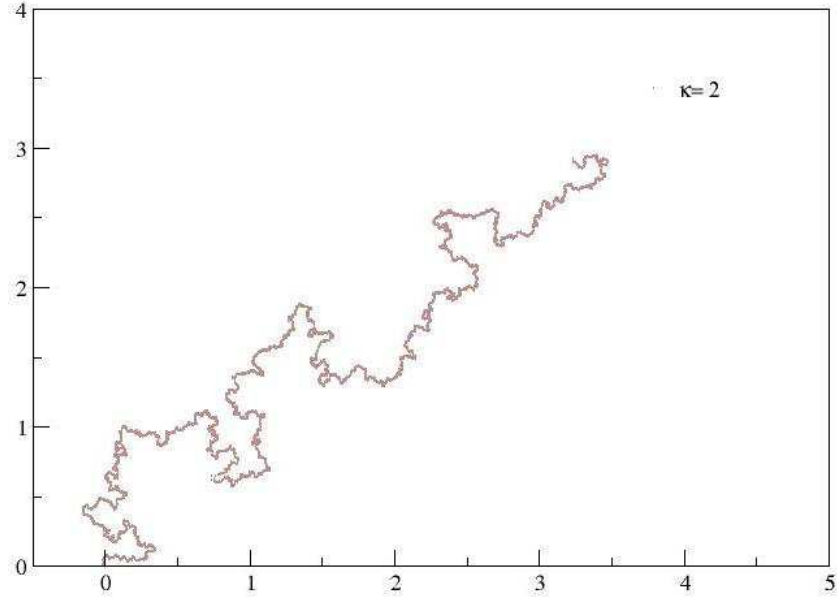


Figure 2. SLE trace for Brownian forcing $\kappa = 2$, 300000 steps, $\tau = 10^{-5}$, $T = 3$

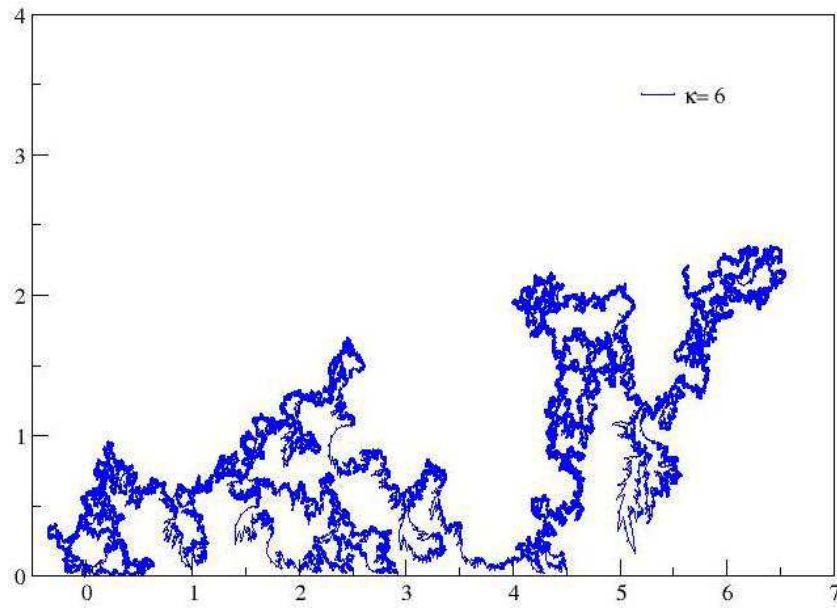


Figure 3. SLE trace for Brownian forcing $\kappa = 6$, 300000 steps, $\tau = 10^{-5}$, $T = 3$

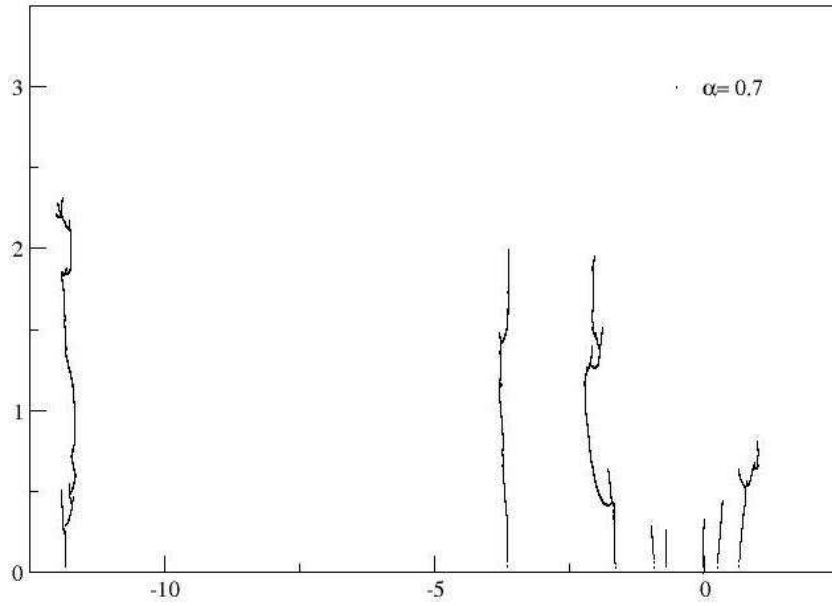


Figure 4. SLE trace for Lévy distributed forcing $\alpha = 0.7$, $c = 4$, 300000 steps, $\tau = 10^{-5}$, $T = 3$

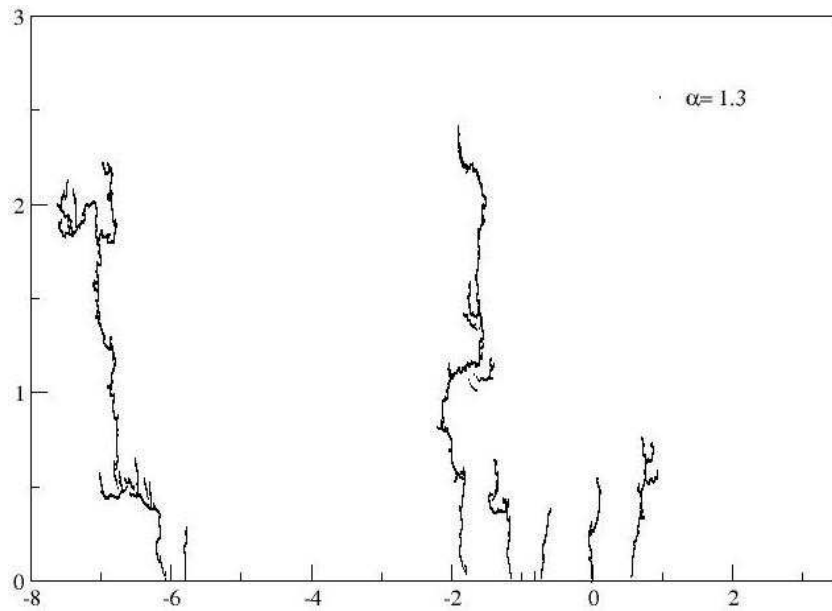


Figure 5. SLE trace for Lévy distributed forcing $\alpha = 1.3$, $c = 4$, 300000 steps, $\tau = 10^{-5}$, $T = 3$

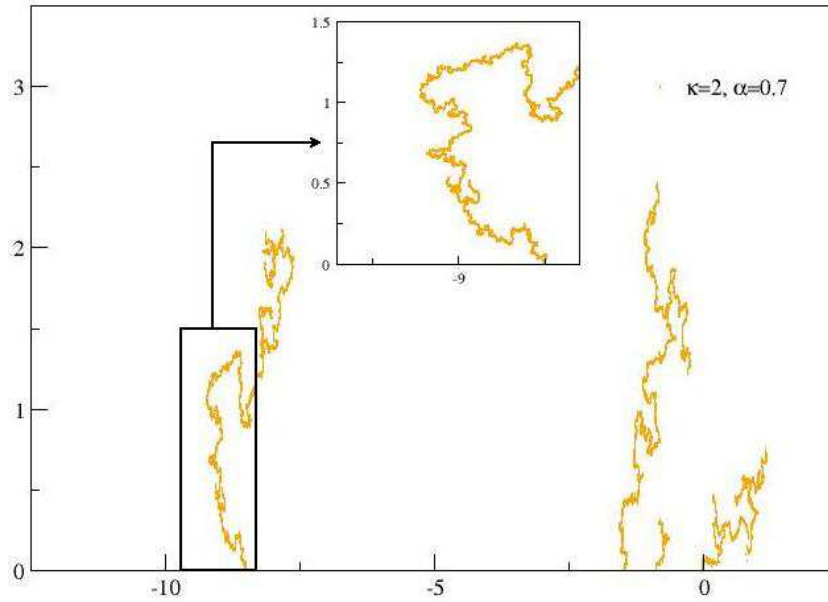


Figure 6. SLE trace with both Lévy flights and Brownian forcing $\alpha = 0.7$, $c = 4$, $\kappa = 2$, 300000 steps, $\tau = 10^{-5}$, $T = 3$, $t^* = 0.17$

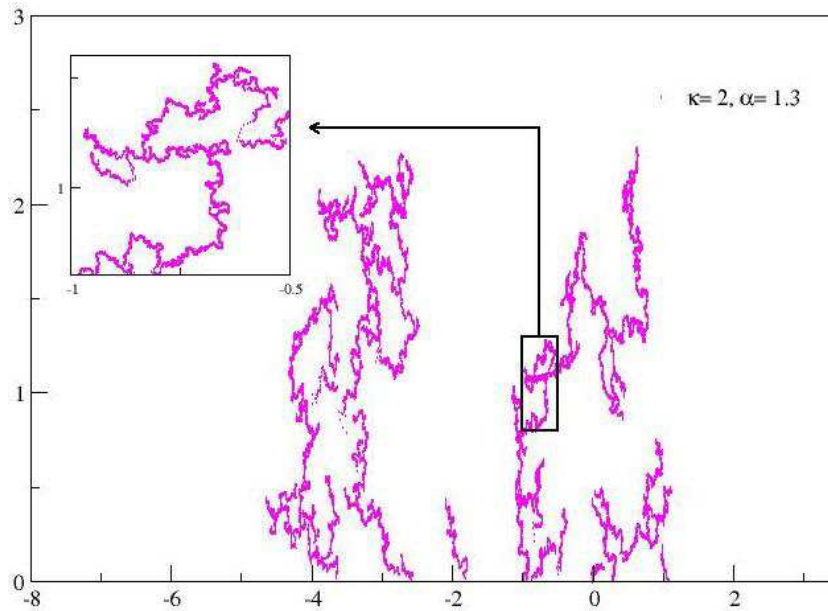


Figure 7. SLE trace with both Lévy flights and Brownian forcing $\alpha = 1.3$, $c = 4$, $\kappa = 2$, 300000 steps, $\tau = 10^{-5}$, $T = 3$, $t^* = 0.31$

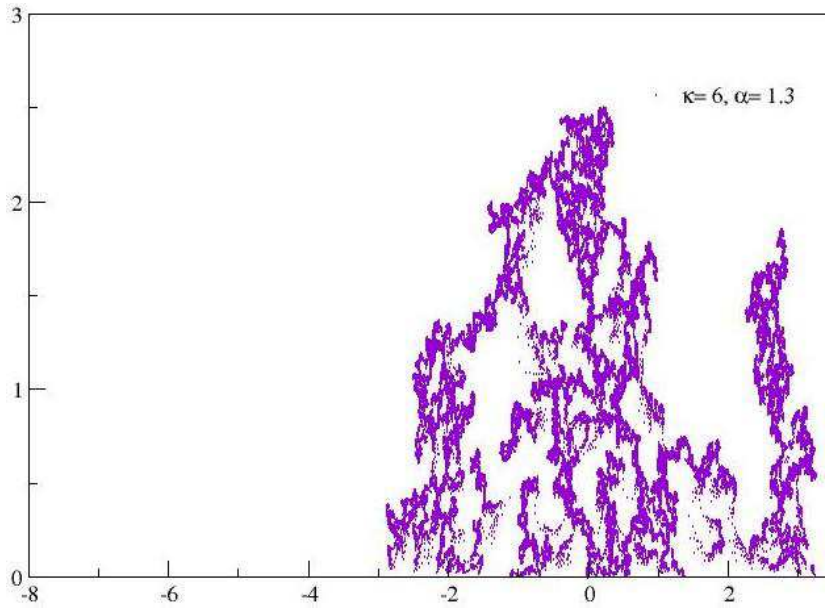


Figure 8. SLE trace with both Lévy flights and Brownian forcing $\alpha = 1.3$, $c = 4$, $\kappa = 6$, 300000 steps, $\tau = 10^{-5}$, $T = 3$, $t^* = 0.07$

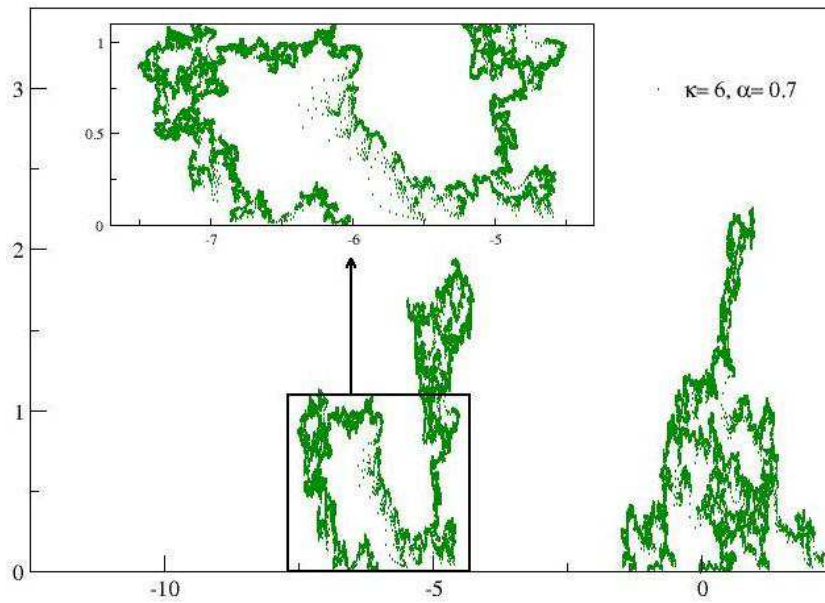


Figure 9. SLE trace with both Lévy flights and Brownian forcing $\alpha = 0.7$, $c = 4$, $\kappa = 6$, 300000 steps, $\tau = 10^{-5}$, $T = 3$, $t^* = 0.53$

is not discussed here. The different behaviors for different values of κ are described as different phases of SLE, basically because the behavior in each interval is qualitatively different from that in the others. The difference is topological in character. It can be seen in both the small- and the large-scale features of the trace. Here we shall discuss phases of the model containing both Brownian and Lévy forcing, but concentrate mostly on small-scale features of touching and near-touching.

Notice that the events when the trace touches the real line and the previously existing parts of itself, are equivalent in the statistical sense, which follows from the stationary increments of the forcing and the composition property of conformal maps. Since the driving force $\xi(t)$ is stationary and SLE is defined by a first-order differential equation, we have the statistical identity

$$h(h(z, s), t) \stackrel{d}{=} h(z, s + t). \quad (20)$$

Consider the trace grown up to a time $s + t$. The part of the trace that developed earlier (up to time s) can be mapped to the real axis by $h(z, s)$. Then the event of the growing hull swallowing (or coming arbitrarily close to swallowing) a point somewhere on its previously grown boundary is statistically equivalent to the event of the hull swallowing (or almost swallowing) a point on the real axis, and the probabilities of such events should be the same. Therefore, to determine the probability of swallowing for points anywhere on the boundary of the hull, it is enough to determine the probability of swallowing only for the points on the real axis. This was initially argued for purely Brownian SLE, and remains valid here.

3.2. Using Dynkin's formula

The main tool that we will use to determine phase transitions in SLE is Dynkin's formula [21, 22]. It can be written for a generic stochastic process (not necessarily Lévy), but we will restrict it to Lévy processes and stochastic integrals of them, that is, processes $X(t)$ defined by a Langevin-like equation

$$\partial_t X_t = F(X(t)) + \partial_t(\text{Lévy process}), \quad (21)$$

with any drift function F . Dynkin's formula gives the average value of any function f of the stochastic process $X(t)$ at an exit time T :

$$\langle f(X(T)) \rangle = f(x_0) + \left\langle \int_0^T Af(X(t)) dt \right\rangle. \quad (22)$$

Here x_0 is the initial value of the process: $X(0) = x_0$, and A is the generator of the process, that is, the operator acting on the argument of the function f and representing time differentiation. By choosing $f(x)$ to be a zero mode of the generator:

$$Af(x) = 0, \quad (23)$$

we get rid of the integral term. Note that we may solve (23) with any boundary condition: any non-constant solution is sufficient. In the Brownian case this equation is differential and easy to solve. Thus, Dynkin's formula produces many results about Brownian motion, such as recurrence, transience, etc. [21].

3.3. Brownian forcing

As an example of using Dynkin's formula we first derive the phase transition at $\kappa = 4$ for purely Brownian SLE. This calculation is usually done in literature with the aid of martingales [4].

Let us set $c = 0$ in Eq. (7). As a function of time, $h(z, t)$ is a continuous stochastic process with the initial condition $h(z, 0) = z$. The event in which z is swallowed by the hull at a time T corresponds to the event $h(z, T) = 0$ on the mathematical plane. We choose z to be on the real axis in the physical plane, then $h(z, t)$ is real.

Let us consider a real $x > 0$ for concreteness. On the mathematical plane, we fix points a and b on the real axis so that

$$0 < a < x < b < \infty. \quad (24)$$

Let T be the exit time from the interval $[a, b]$. Being continuous, the process $h(x, t)$ can exit $[a, b]$ either through a (with probability p_a), or through b (with probability $1 - p_a$). Clearly, $h(x, T)$ is either a , or b . Then Dynkin's formula becomes

$$p_a f(a) + (1 - p_a) f(b) = f(x), \quad (25)$$

and allows us to find p_a , the probability for $h(x, t)$ to hit a before hitting b . Now if we take the limits $a \rightarrow 0$, $b \rightarrow \infty$, it becomes the probability for $h(x, t)$ to hit 0 in a finite time, which is the probability for the point x on the physical plane to be swallowed by the hull:

$$p = \lim_{b \rightarrow \infty} \lim_{a \rightarrow 0} \frac{f(x) - f(b)}{f(a) - f(b)}. \quad (26)$$

In general, the order of limits matters here. If it is reversed,

$$\tilde{p} = \lim_{a \rightarrow 0} \lim_{b \rightarrow \infty} \frac{f(x) - f(b)}{f(a) - f(b)} \quad (27)$$

is the probability for $h(z, t)$ to come arbitrarily close to 0, that is, for the hull to come arbitrarily close to the boundary.

The generator for the process $h(z, t)$ driven by the Brownian motion (4) is [21]

$$A_B = \frac{2}{x} \partial_x + \frac{\kappa}{2} \partial_x^2. \quad (28)$$

A zero mode of this operator is

$$f_B(x) = \begin{cases} |x|^{1-\frac{4}{\kappa}} & \text{for } \kappa \neq 4, \\ \log |x| & \text{for } \kappa = 4. \end{cases} \quad (29)$$

Substituting this into Eqs. (26, 27) we find that the answer is independent of z , thus the probability for the hull to touch the boundary

$$p_{c=0} = \begin{cases} 0 & \text{for } \kappa \leq 4, \\ 1 & \text{for } \kappa > 4. \end{cases} \quad (30)$$

For $\kappa = 4$ the order of limits is important and we find that

$$\tilde{p}_{c=0} = \begin{cases} 0 & \text{for } \kappa < 4, \\ 1 & \text{for } \kappa \geq 4. \end{cases} \quad (31)$$

Note that in order to determine the phases, only the behavior of a zero mode of A at zero and at infinity is necessary. Examples of traces of standard SLE are shown in Figures 2 and 3. Touching is visible for the $\kappa = 6$ and apparently does not occur for $\kappa = 2$.

3.4. Dynkin's formula with Lévy flights

The case of the generalized SLE is different from the Brownian case: now $h(z, t)$ has discontinuities. Therefore, at the exit time T the value of $h(z, T)$ does not have to be a or b : the process can jump and overshoot the boundary of the interval. To avoid this difficulty, we define T to be the exit time from the set

$$S = [-b, a) \cup (a, b], \quad (32)$$

and also restrict ourselves to zero modes that are even functions of x .

The process $h(z, t)$ can exit S by either hitting a (no overshooting possible), or by taking a value beyond $-b$ or b , in which case the overshooting is possible. But we consider the limit $b \rightarrow \infty$. The behavior of zero modes, considered below, is simple at infinity: they either diverge or are constant. With these changes complete, we return to Eqs. (26, 27).

The generator for the process $h(z, t)$ defined by Eqs. (2, 7) is (see [10]) $A = A_B + A_L$, where A_B is the same as in Eq. (28), and

$$A_L f(x) = -\frac{c}{2\Gamma(-\alpha) \cos \frac{\pi\alpha}{2}} \int (f(x+y) - f(x)) \frac{dy}{|y|^{1+\alpha}}. \quad (33)$$

This operator contains the principal value integral, which ensures convergence at small y for $\alpha < 2$. The meaning of this term is most transparent in the Fourier space, where it is equivalent to the multiplication by $-c|k|^\alpha$.

Once again, we need to find a zero mode $f(x)$, obeying $Af = 0$. These zero modes are studied in detail in the Appendix. Here we summarize the results.

First of all, we find by direct calculation that the function

$$f_L(x) = \begin{cases} |x|^{\alpha-1}, & \alpha \neq 1, \\ \ln|x|, & \alpha = 1 \end{cases} \quad (34)$$

is a zero mode of A_L . Comparing this with Eq. (29), we conclude that $f_B(x) = f_L(x)$ if $1 - 4/\kappa = \alpha - 1$, or

$$\alpha = 2 - \frac{4}{\kappa}. \quad (35)$$

Along this line on the phase diagram we have an explicit expression for a zero mode of the full operator A .

Secondly, for arbitrary α and κ we can transform the zero mode equation, $Af = 0$, into Fourier space:

$$\frac{d}{dk} \left[(c|k|^\alpha + \frac{\kappa}{2}k^2) \tilde{f}(k) \right] - 2k\tilde{f}(k) = 0, \quad (36)$$

where $\tilde{f}(k)$ is the Fourier transform of $f(x)$. A solution of this equation is

$$\tilde{f}(k) = |k|^{-\alpha} \left(1 + \frac{\kappa}{2c} |k|^{2-\alpha} \right)^{\frac{4}{(2-\alpha)\kappa} - 1}. \quad (37)$$

Apart from a multiplicative constant and a possible delta function at $k = 0$, this solution is unique. Its asymptotic behavior is

$$\tilde{f}(k) \sim \begin{cases} |k|^{\frac{4}{\kappa} - 2}, & k \rightarrow \infty, \\ |k|^{-\alpha}, & k \rightarrow 0. \end{cases} \quad (38)$$

Note that Brownian motion determines the behavior at large k (small distances in x -space), whereas Lévy flights determine the behavior at small k (large distances in x -space).

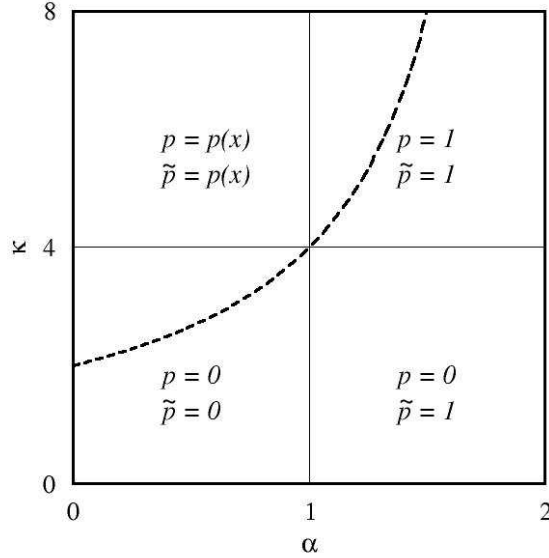


Figure 10. The phase diagram of the generalized SLE (9). The dashed line is the hyperbola given by Eq. (35) in the text. Along this line an explicit expression for the zero mode of the generator A is known, see Eq. (34).

Analysis of the asymptotic behavior of the inverse Fourier transform of Eq. (37) gives the following:

$$f(x) \sim \begin{cases} |x|^{1-\frac{4}{\kappa}} & \text{for } \kappa \neq 4 \text{ and } x \rightarrow 0, \\ \log |x| & \text{for } \kappa = 4 \text{ and } x \rightarrow 0, \\ |x|^{\alpha-1} & \text{for } \alpha \neq 1 \text{ and } x \rightarrow \infty, \\ \log |x| & \text{for } \alpha = 1 \text{ and } x \rightarrow \infty. \end{cases} \quad (39)$$

Strictly speaking, we are able to obtain these asymptotics only for $\kappa > 2$. The trouble is that the function that behaves as $|x|^{1-4/\kappa}$ with $\kappa < 2$ for small x would lead to a divergent integral in Eq. (33), and so cannot be a zero mode of A . Nevertheless, on physical grounds we believe that there is nothing special happening at $\kappa = 2$, and that our results for phases that we state next, apply to all values $\kappa > 0$.

The use of the asymptotic behavior (39) in the formulas (26, 27) gives the phases of SLE driven by the noise (7):

- **isolated trees** $\kappa \leq 4, \alpha < 1$: $p = 0, \tilde{p} = 0$. An example of the trace is shown in Figure 6. The Lévy flights have broad distribution. Long jumps occur often. The trace can jump far from the existing trees and then a new isolated tree starts growing. The chances of returning to one of the old trees are small, so the old trees stop growing. We hope to make this point quantitatively in a future publication.
- **a forest of trees** $\kappa \leq 4, 1 \leq \alpha < 2$: $p = 0, \tilde{p} = 1$. An example of the trace is shown in Figure 7. The Lévy flights rarely produce very big jumps, so that the trace starts a new tree close to the old one, or does not leave the old tree at all. The hull looks like trees growing close to each other with their branches almost touching.

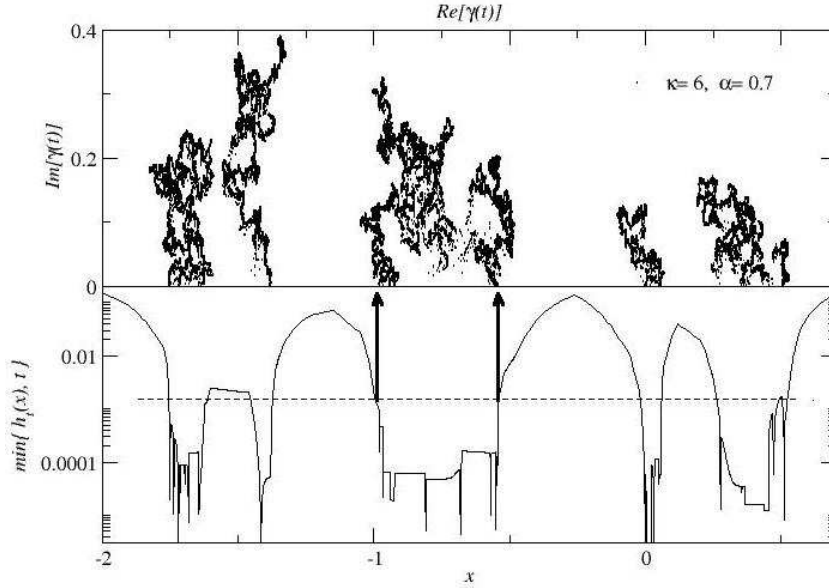


Figure 11. We calculate which points on the real axis plane have been swallowed by calculating $H(x) = \min\{h(x, t); t < T\}$. There is a direct correspondence between the areas swallowed by the trace on the physical plane and the process $h(x, t)$ on the mathematical plane.

- **a forest of bushes** $\kappa > 4$, $1 \leq \alpha < 2$: $p = 1$, $\tilde{p} = 1$. An example of the trace is shown in Figure 8. The Brownian motion, which controls the small scales, is stronger now. The trees become thicker and different branches touch each other.
- **isolated bushes** $\kappa > 4$, $\alpha < 1$: p and \tilde{p} are equal and finite, that is, the probability for a fixed point x on the real axis to be swallowed by the hull at a finite time is a function $p(x)$ of the position of this point. This function is defined by any of the equations (26, 27) (the order of limits is unimportant in this phase), where $f(x)$ is the inverse Fourier transform of (37). $p(x)$ is a symmetric function decaying from $p(0) = 1$ to $p(\infty) = 0$ with the asymptotic behavior:

$$p(x) \sim |x|^{\alpha-1} \quad \text{for } x \rightarrow \infty, \quad 1 - p(x) \sim |x|^{1-\frac{4}{\kappa}} \quad \text{for } x \rightarrow 0. \quad (40)$$

An example of the trace is shown in Figure 9. Since $p(x)$ varies between 0 and 1, parts of the real axis will not be swallowed, leaving gaps among trees.

As long as $c > 0$, the first three phases do not depend on c at all. This is an expected property, because unlike κ and α , c flows under the renormalization (11) and p and \tilde{p} are constants. A phase diagram of the generalized SLE is shown in Fig. 10.

3.5. Probability $p(x)$ of swallowing on the real axis

Figures 3, 9 and 8 seem to show that the trace swallows whole areas and touches itself. In the numerical approximation where the forcing consists of discontinuous steps the trace doesn't exactly touch itself, however it comes closer to touching as $\tau \rightarrow 0$ and whole areas thus appear to be swallowed. We can then try to determine the probabilities for swallowing by setting a small-distance cut-off and looking for limiting behavior as the cut-off goes to zero.

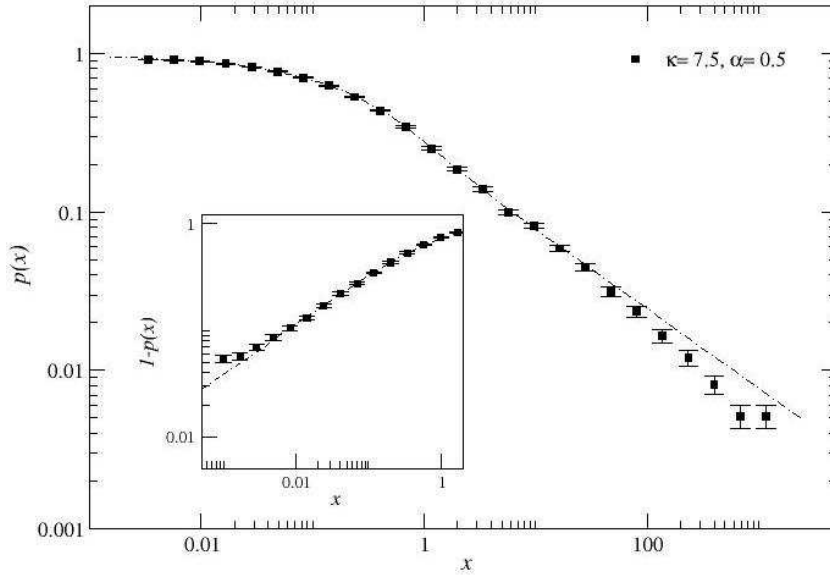


Figure 12. SLE with Lévy Flights and Brownian component ($\kappa = 7.5, \alpha = 0.5, c = 10$). Main - Large x behavior: Probability $p(x)$ of a point x on the real axis not to be swallowed until time $T = 10$ ($\tau = 10^{-5}$, 1000000 steps, $t^* = 0.09$, $H_c = 3 \cdot 10^{-3}$, statistics for 7000 independent noise realizations). Inset - Small x behavior: Probability $1 - p(x)$ ($\tau = 10^{-6}$, 1000000 steps, $H_c = 6 \cdot 10^{-4}$, statistics for 3000 independent noise realizations). In both cases the dotted line is the theoretical prediction (Eq. (39)) which is followed accurately by the numerics for four decades of x . Deviations for small $x < 0.003$ are due to the finite time step τ of the noise realizations; the data points approach the theoretical prediction as we approach the scaling limit (not shown)

In order to measure $p(x)$ we consider the real stochastic process $h(x, t)$ on the mathematical plane defined by Eq. (2). A point x on the axis is considered to be swallowed at time T if $|h(x, t)| < H_c$ for some $t < T$. Our method for determining H_c is shown in Figure 11: For one particular realization of the noise we calculate $H(x) = \min\{|h(x, t)|, t \leq T\}$ for x on the real axis. We use the same realization to draw the trace on the physical plane. From the trace we can infer which points of the axis have been surrounded by the curve and thus have been swallowed. In the figure the boundaries of a swallowed area on the real axis are marked by the arrows; the dashed line corresponds to the cut off H_c , we see that all points at which $H(x) < H_c$ appear to be swallowed in the physical plane. We repeat for several noise realizations to determine the value of the cut off accurately. The existence of the cut-off means we will be unable to distinguish between p and \tilde{p} , so that the case $\alpha > 1, \kappa < 4$ (the forest of trees) will be similar to $\alpha > 1, \kappa > 4$ (the forest of bushes). For all cases we have taken $T \gg t^* = \left(\frac{\kappa^\alpha}{c^2}\right)^{1/(2-\alpha)}$.

Figure 12 shows the results of the probability distribution $p(x)$ of a point on the real axis being swallowed by the time $T = 10$ for a case with $\alpha < 1, \kappa > 4$ (isolated bushes). The numerical results closely follow the theoretical prediction of Eq. (40).

In general, we reproduce the theoretical form of $p(x)$ rather well in this phase, but less well in the other phases. This is not surprising, it is the effect of finite time T in

our calculation. In the phases with forests, points are surrounded by a process which includes multiple returns to the same region of x . In the simulations, not enough time is allowed for this multiple return to work itself out. Furthermore, our use of the cut-off means we are unable to distinguish between p and \tilde{p} , so that the method makes the forest of trees look similar to the forest of bushes. Thus, we shall have to put together a more refined method of analysis and do much longer runs to make this distinction.

Discussion and conclusions

The generalization of stochastic Loewner evolution, suggested in this paper, has many new features. The hull acquires branching and the growth becomes a tree-like stochastic process. The phases of such hull are very different from the usual SLE. Although the driving force of SLE is still self-similar, the growing hull is not, the force of the Lévy flights increases with time, being a relevant parameter under size rescaling.

The non-stationary nature of the growth considered in this paper is related to a technical difficulty in its study. Many properties of the standard SLE are obtained using the so-called random time change which, in the case of the Brownian forcing, is consistent with the form of the Loewner equation (1). In the case of Lévy processes a similar random time change exists, but changes the nature of the Loewner equation (9) and, therefore, cannot be used to extract useful information.

In terms of the geometry of the generalized SLE driven by Lévy processes, the non-stationarity means that many such properties as, for example, the fractal dimension of the trace cannot be globally defined. Instead, they may possibly be defined locally at each stage of the evolution. The question of how one can characterize the geometry of the generalized SLE will be addressed in a future publication.

Acknowledgments

This research was supported in part by NSF MRSEC Program under DMR-0213745. IG is an Alfred P. Sloan Research Fellow, and was also supported by an award from Research Corporation and the NSF Career Award under DMR-0448820. We wish to acknowledge many helpful discussions with Paul Wiegmann, Eldad Bettelheim, and Seung Yeop Lee. IG also acknowledges useful communications with John Cardy and Nigel Goldenfeld.

Appendix

In this Appendix we study zero modes of the operator $A = A_B + A_L$, where

$$A_B = \frac{2}{x}\partial_x + \frac{\kappa}{2}\partial_x^2, \quad A_L f(x) = C \int \frac{f(y+x) - f(x)}{|y|^{1+\alpha}} dy. \quad (\text{A.1})$$

Direct approach

A zero mode of A_B is given in Eq. (29). To find zero modes of A_L , let us consider the integral

$$I_{\alpha,\beta}(x) = \int \frac{|y+x|^\beta - |x|^\beta}{|y|^{1+\alpha}} dy. \quad (\text{A.2})$$

This integral converges at large y if $\beta < \alpha$, at small y for any β and any $\alpha < 2$ (because of the principal value), and at $y \approx -x$ for $\beta > -1$. Thus, we assume $-1 < \beta < \alpha < 2$.

By rescaling $y \rightarrow |x|y$ we reduce the integral (A.2) (for nonzero x) to

$$I_{\alpha,\beta}(x) = I_{\alpha,\beta} |x|^{\beta-\alpha}, \quad I_{\alpha,\beta} = \int \frac{|y+1|^\beta - 1}{|y|^{1+\alpha}} dy. \quad (\text{A.3})$$

The last integral here can be evaluated. First, we split the integration interval into three intervals and change variables in each appropriately:

$$\begin{aligned} I_{\alpha,\beta}^\epsilon &= \left(\int_{-\infty}^{-1} + \int_{-1}^{-\epsilon} + \int_{\epsilon}^{\infty} \right) \frac{|y+1|^\beta - 1}{|y|^{1+\alpha}} dy \\ &= \int_1^{\infty} \frac{(y-1)^\beta - 1}{y^{1+\alpha}} dy + \int_{\epsilon}^1 \frac{(1-y)^\beta - 1}{y^{1+\alpha}} dy + \int_{\epsilon}^{\infty} \frac{(y+1)^\beta - 1}{y^{1+\alpha}} dy. \end{aligned}$$

The integrals here can be found in Ref. [23]. Some of them contain hypergeometric functions that have to be transformed further by applying the Kummer's connection formulas (see Sec. 2.9. in Chapter 2 of Ref. [24]). Combining all the results, we obtain

$$\begin{aligned} I_{\alpha,\beta}^\epsilon &= \frac{\Gamma(\beta+1)\Gamma(\alpha-\beta)}{\Gamma(\alpha+1)} + \frac{\Gamma(\beta+1)\Gamma(-\alpha)}{\Gamma(\beta-\alpha+1)} + \frac{\Gamma(\alpha-\beta)\Gamma(-\alpha)}{\Gamma(-\beta)} \\ &\quad + \frac{1}{\alpha} \epsilon^{-\alpha} ({}_2F_1(-\alpha, -\beta; 1-\alpha; \epsilon) + {}_2F_1(-\alpha, -\beta; 1-\alpha; -\epsilon) - 2). \end{aligned}$$

Finally, in the limit $\epsilon \rightarrow 0$, the last term here vanishes, and we get

$$I_{\alpha,\beta} = \frac{\Gamma(\beta+1)\Gamma(\alpha-\beta)}{\Gamma(\alpha+1)} + \frac{\Gamma(\beta+1)\Gamma(-\alpha)}{\Gamma(\beta-\alpha+1)} + \frac{\Gamma(\alpha-\beta)\Gamma(-\alpha)}{\Gamma(-\beta)}. \quad (\text{A.4})$$

Note that this expression vanishes identically if $\beta = \alpha - 1$, thus showing that $f_L(x) = |x|^{\alpha-1}$ is a zero mode of A_L .

Let us now consider the limit of $\beta \rightarrow 0$. Specifically, we note that

$$\begin{aligned} J_\alpha(x) &= \lim_{\beta \rightarrow 0} \beta^{-1} I_{\alpha,\beta}(x) = \int \frac{\ln \left| \frac{y}{x} + 1 \right|}{|y|^{1+\alpha}} dy = J_\alpha |x|^{-\alpha}, \\ J_\alpha &= \int \frac{\ln |y+1|}{|y|^{1+\alpha}} dy. \end{aligned} \quad (\text{A.5})$$

The last integral can be obtained from Eq. (A.4) by carefully taking the limit $\beta \rightarrow 0$. Expanding gamma functions we get

$$\beta^{-1} I_{\alpha,\beta} = \frac{1}{\alpha} (\psi(1-\alpha) - \psi(\alpha)) - \Gamma(\alpha)\Gamma(-\alpha) + O(\beta). \quad (\text{A.6})$$

Finally, using properties of the gamma and digamma functions, we get

$$J_\alpha = \frac{\pi}{\alpha} \cot \frac{\pi\alpha}{2}. \quad (\text{A.7})$$

This expression vanishes at $\alpha = 1$ showing that $f_L(x) = \ln |x|$ is a zero mode of A_L for $\alpha = 1$.

Thus, we have shown that

$$f_L(x) = \begin{cases} |x|^{\alpha-1}, & \alpha \neq 1, \\ \ln |x|, & \alpha = 1 \end{cases} \quad (\text{A.8})$$

is a zero mode of A_L .

Next we note that $f_B(x) = f_L(x)$ if $1 - 4/\kappa = \alpha - 1$ or $\alpha = 2 - 4/\kappa$. Along this line on the phase diagram we have an explicit expression for a zero mode of the full operator A , which behaves for small and large values of x exactly as claimed in the text of the paper. However, this is restricted to the range of $\kappa > 2$ (because α must be positive). This is, actually, more generally true. Indeed, the integral $I_{\alpha,\beta}(x)$ with $\beta = 1 - 4/\kappa$ converges at y near $-x$ only for $\kappa > 2$. Thus, our claims in the paper about the phases can be justified strictly speaking only for $\kappa > 2$.

Fourier transform

After the Fourier transform the zero mode equation $Af = 0$ becomes a differential equation

$$\frac{d}{dk} \left[\left(c|k|^\alpha + \frac{\kappa}{2}k^2 \right) \tilde{f}(k) \right] - 2k\tilde{f}(k) = 0, \quad (\text{A.9})$$

Let us consider $k > 0$. Introducing the new function

$$g(k) = \left(ck^\alpha + \frac{\kappa}{2}k^2 \right) \tilde{f}(k), \quad (\text{A.10})$$

we rewrite the differential equation as

$$\begin{aligned} \frac{dg}{g} &= \frac{2k}{ck^\alpha + \frac{\kappa}{2}k^2} dk = \frac{2k^{1-\alpha}}{c + \frac{\kappa}{2}k^{2-\alpha}} dk \\ &= \frac{4}{(2-\alpha)\kappa} d \ln \left(c + \frac{\kappa}{2}k^{2-\alpha} \right). \end{aligned} \quad (\text{A.11})$$

This is immediately integrated to give

$$g(k) = \left(c + \frac{\kappa}{2}k^{2-\alpha} \right)^{\frac{4}{(2-\alpha)\kappa}}. \quad (\text{A.12})$$

The case $k < 0$ is treated similarly, and we get in the end an even function (as expected):

$$\tilde{f}(k) = |k|^{-\alpha} \left(c + \frac{\kappa}{2}|k|^{2-\alpha} \right)^{\frac{4}{(2-\alpha)\kappa} - 1}. \quad (\text{A.13})$$

Apart from a multiplicative constant and a possible delta function at $k = 0$, this solution is unique.

Performing the inverse Fourier transform, we obtain a representation of our zero mode:

$$f(x) = \int_{-\infty}^{\infty} \frac{dk}{2\pi} e^{ikx} \tilde{f}(k) = \frac{1}{\pi} \int_0^{\infty} dk \cos(kx) \tilde{f}(k). \quad (\text{A.14})$$

This integral diverges at the lower limit for $\alpha > 1$, but this is a spurious divergence that is easy to amend. Namely, we can formally subtract a (possibly infinite) constant from $f(x)$ replacing it by

$$f(x) = \frac{1}{\pi} \int_0^{\infty} dk (\cos(kx) - 1) \tilde{f}(k) = \frac{2}{\pi} \int_0^{\infty} dk \sin^2 \left(\frac{kx}{2} \right) \tilde{f}(k). \quad (\text{A.15})$$

This integral converges at the lower limit for all values $\alpha < 2$, which is all we need.

Situation with convergence at the upper limit is trickier. By Chartier's criterion (see Ref. [25]), the integral (A.14) converges at the upper limit only if $\kappa > 2$. This is the same condition that was obtained in the end of the previous subsection where the Fourier transform was not used at all. So, this seems to be a more problematic issue.

We also note that after the subtraction performed in Eq. (A.15), the convergence at the upper limit worsens. Now the integral is convergent only for $\kappa > 4$. But this can be ignored. We simply perform the integration for $\kappa > 4$ and then analytically continue to smaller values of κ . Convergence also improves when we take derivative in either of Eqs. (A.14, A.15) with respect to the strength of the Lévy term c . We can then in principle obtain $f(x)$ integrating in c .

Another comment is in order here. If we tried to obtain the zero mode $f_B(x)$ for the Brownian SLE case using the Fourier transform, we would get

$$f(x) = \int_{-\infty}^{\infty} \frac{dk}{2\pi} e^{ikx} |k|^{\frac{4}{\kappa}-2} = \frac{1}{\pi} \int_0^{\infty} dk \cos(kx) k^{\frac{4}{\kappa}-2} \quad (\text{A.16})$$

instead of Eq. (A.14). The last integral has the same behavior at infinity as the one in Eq. (A.14). But the zero mode $f_B(x)$ of A_B given in Eq. (29) exist for all values of κ . This is another reason for us to believe that the value $\kappa = 2$ is not special, and that our results for the phases of the generalized SLE apply for all values of κ .

Consider now the integral

$$f(x, \kappa, \alpha) = \int_0^{\infty} dk k^{-\alpha} \left(1 + k^{2-\alpha}\right)^{\frac{4}{(2-\alpha)\kappa}-1} \sin^2\left(\frac{kx}{2}\right), \quad (\text{A.17})$$

where we ignored the overall constant coming from pulling a power c out of the integral, as well as rescaling of k and x . This integral can be evaluated explicitly through hypergeometric functions for such values of α that

$$2 - \alpha = \frac{2p}{q}, \quad (\text{A.18})$$

where $p, q \in \mathbb{N}$ are mutually prime, see Ref. [23], Eq. 2.5.2.3. The Mathematica software can also do the integral with these values of α . The simplest of these corresponds to $p = 1, q = 2$, that is, $\alpha = 1$. The corresponding integral is

$$\begin{aligned} f(x, \kappa, 1) &= \int_0^{\infty} dk k^{-1} (1+k)^{\frac{4}{\kappa}-1} \sin^2\left(\frac{kx}{2}\right) \\ &= \frac{\pi \sec\left(\frac{2\pi}{\kappa}\right)}{4\Gamma\left(2 - \frac{4}{\kappa}\right)} {}_1F_2\left(\frac{1}{2} - \frac{2}{\kappa}; \frac{1}{2}, \frac{3}{2} - \frac{2}{\kappa}; -\frac{x^2}{4}\right) x^{1-\frac{4}{\kappa}} \\ &\quad - \frac{\pi \kappa \csc\left(\frac{2\pi}{\kappa}\right)}{8(\kappa-2)\Gamma\left(\frac{\kappa-4}{\kappa}\right)} {}_1F_2\left(1 - \frac{2}{\kappa}; \frac{3}{2}, 2 - \frac{2}{\kappa}; -\frac{x^2}{4}\right) x^{2-\frac{4}{\kappa}} \\ &\quad + \frac{\kappa^2}{16(\kappa+4)} {}_2F_3\left(1, 1; 2, 1 + \frac{2}{\kappa}, \frac{3}{2} + \frac{2}{\kappa}; -\frac{x^2}{4}\right) x^2. \quad (\text{A.19}) \end{aligned}$$

For all values of α given by Eq. (A.18) the structure of the answers is similar. They are given in terms of hypergeometric functions ${}_pF_q$. The asymptotic analysis of these expressions can be performed with the help of Ref. [26], and in all cases gives the result given in Eq. (39).

References

- [1] B. Nienhuis in *Phase transitions and critical phenomena*, vol. 11, C. Domb and J. L. Lebowitz, eds., Academic Press, 1987.
- [2] B. Duplantier, Phys. Rev. Lett. **84**, 1363 (2000); *Conformal fractal geometry and boundary quantum gravity*, in *Fractal geometry and applications: a jubilee of Benoit Mandelbrot, Part 2*, 365, Proc. Sympos. Pure Math., 72, Part 2, Providence, RI: American Mathematical Society, 2004; arXiv: math-ph/0303034.

- [3] O. Schramm, *Israel J. Math.*, **118**, 221 (2000); arXiv: math.PR/9904022.
- [4] S. Rohde and O. Schramm, arXiv: math.PR/0106036.
- [5] G. F. Lawler. *Conformally invariant processes in the plane*. Mathematical Surveys and Monographs, **114**. American Mathematical Society, 2005.
- [6] W. Werner, *Random planar curves and Schramm-Loewner evolutions*, in *Lecture Notes in Mathematics*, **1840**. Springer-Verlag, 2004; arXiv: math.PR/0303354.
- [7] W. Kager and B. Nienhuis, *J. Stat. Phys.* **115**, 1149 (2004); arXiv: math-ph/0312056.
- [8] J. Cardy, *Ann. Phys.* **318**, 81 (2005); arXiv: cond-mat/0503313
- [9] L. V. Ahlfors, *Conformal invariants: topics in geometric function theory*, New York, McGraw-Hill, 1973.
- [10] D. Applebaum, *Lévy processes and stochastic calculus*, Cambridge University Press, 2004.
- [11] K.-I. Sato, *Lévy processes and infinitely divisible distributions*, Cambridge University Press, 1999.
- [12] G. Samorodnitsky, M. Taqqu, *Stable non-Gaussian random processes: stochastic models with infinite variance*, New York: Chapman & Hall, 1994.
- [13] R. Metzler, J. Klafter, *Phys. Rep.* **339**, 1 (2000).
- [14] D. Marshall and S. Rohde, *J. Amer. Math. Soc.* **18**, 763 (2005).
- [15] W. Kager, B. Nienhuis, L. P. Kadanoff, *J. Stat. Phys.* **115**, 805 (2004).
- [16] J. R. Lind, *Ann. Acad. Sci. Fenn. Math.* **30**, 143 (2005).
- [17] V. Beffara, arXiv: math.PR/0211322.
- [18] M. B. Hastings, *Phys. Rev. Lett.* **88**, 055506 (2002); arXiv: cond-mat/9607021.
- [19] L. P. Kadanoff, M. K. Berkenbusch, *Nonlinearity* **17**, R41 (2004); **18**, 937 (2005).
- [20] J. M. Chambers, C. L. Mallows, B. W. Stuck. *J. Amer. Statist. Assoc.* **71**, 340 (1976).
- [21] B. Øksendal, *Stochastic differential equations: an introduction with applications*, Springer, 1992.
- [22] *Encyclopedic Dictionary of Mathematics*, MIT Press, Cambridge, Massachusetts, 1993, article “Markov Processes”, p. 974.
- [23] A. P. Prudnikov, Yu. A. Brychkov, O. I. Marichev, *Integrals and series*, vol. 1, New York, Gordon and Breach Science Publishers, 1986.
- [24] H. Bateman, A. Erdélyi, *Higher Transcendental Functions*, vol. 1, New York, McGraw-Hill, 1953.
- [25] E. H. Whittaker and G. N. Watson, *A course of modern analysis*, section 4.43 (IV), New York, AMS Press, 1979.
- [26] Y. L. Luke, *Mathematical functions and their approximations*, New York, Academic Press, 1975; *The special functions and their approximations*, New York, Academic Press, 1969.